


# Synchrotron-Based Three-Dimensional Fourier-Transform Infrared Spectro-Microtomography of Murchison Meteorite Grain

Mehmet Yesiltas<sup>1,2</sup>, Julia Sedlmair<sup>3,4</sup>, Robert E. Peale<sup>1</sup>, and Carol J. Hirschmugl<sup>5</sup>

Applied Spectroscopy  
2017, Vol. 71(6) 1198–1208  
© The Author(s) 2016  
Reprints and permissions:  
sagepub.co.uk/journalsPermissions.nav  
DOI: 10.1177/0003702816671072  
journals.sagepub.com/home/asp  


## Abstract

We demonstrate nondestructive, three-dimensional, microscopic, infrared (IR) spectral in-situ imaging of an extraterrestrial sample. Spatially resolved chemical composition and spatial correlations are investigated within a single 45  $\mu\text{m}$  grain of the Murchison meteorite. Qualitative and quantitative investigation through this analytical technique can help elucidate the origin and evolution of meteoritic compounds as well as parent body processes without damaging or altering the investigated samples.

## Keywords

Fourier transform infrared spectroscopy, FT-IR, synchrotron-based FT-IR imaging, tomography, meteorites, Murchison

Date received: 13 April 2015; accepted: 20 June 2016

## Introduction

Meteorites are samples of asteroids, comets, and other planetary bodies such as the Moon and Mars. Various extraterrestrial processes (e.g., thermal metamorphism, aqueous alteration, shocks, and weathering) affect chemical compositions of meteorites. Whether they are interstellar, nebular, or asteroidal processes, primitive meteorites contain signatures of these events in their composition.<sup>1</sup> The study of organic matter, their distribution, and spatial relationships in meteorites are especially of interest. Understanding these organic-mineral associations is key to understanding processes and mechanisms for the formation of organic matter in the early solar system.<sup>2</sup> Evidence suggests that organic matter may have been selectively formed on specific mineral surfaces through catalytic reactions.<sup>2–13</sup> Therefore, a genetic link between the host mineral species and the produced organic matter is highly possible. However, these relations remain poorly understood.

Carbonaceous chondrites, the most primitive meteorites,<sup>14</sup> are highly heterogeneous extraterrestrial samples with up to ~5 wt% carbon.<sup>15</sup> Their chemical composition contains a variety of organics and minerals of complex origin and evolutionary history. Knowledge about formation and processing of organic matter remains poor.<sup>16</sup> Investigation of composition and petrology of carbonaceous chondrites

in situ can reveal complex parent body processes and origin of meteorite constituents. For instance, organic compounds in meteorites may have been modified by thermal metamorphism.<sup>17</sup> The majority of organic matter in carbonaceous chondrites is insoluble<sup>18</sup> and their spatial associations with minerals may provide insights on their formation mechanisms.<sup>19</sup>

Existing analytical techniques to characterize meteorite constituents include infrared (IR),<sup>20,21</sup> Raman,<sup>22,23</sup> and X-ray<sup>24</sup> spectroscopies, nuclear magnetic resonance,<sup>25,26</sup> and carbon X-ray absorption near-edge structure spectroscopy.<sup>27,28</sup> Among these, IR spectroscopy has been the most widely employed for investigating chemical composition.

<sup>1</sup>Department of Physics, University of Central Florida, Orlando, Florida, USA

<sup>2</sup>Department of Geosciences, Stony Brook University, Stony Brook, New York, USA

<sup>3</sup>Forest Products Laboratory, US Department of Agriculture Forest Service, Madison, Wisconsin, USA

<sup>4</sup>Bruker AXS, Madison, Wisconsin, USA

<sup>5</sup>Department of Physics, University of Wisconsin-Milwaukee, Milwaukee, Wisconsin, USA

## Corresponding author:

Mehmet Yesiltas, Department of Physics, University of Central Florida, Orlando, FL 32816, USA.

Email: myesiltas@knights.ucf.edu

Sandford et al.<sup>29</sup> found that organics in comet 81P/Wild 2 samples have a heterogeneous and unequilibrated distribution. Beck et al.<sup>1</sup> investigated asteroidal processes through IR transmission spectroscopy of carbonaceous chondrites. Using mid-IR spectroscopy, Morlok et al.<sup>30</sup> compared achondrites to astronomical observations of dust in protoplanetary disks.

We previously demonstrated that organics and minerals can be mapped in situ in meteorites by two-dimensional (2D) IR spectral microscopic imaging,<sup>19,31–33</sup> which revealed organic-mineral relationships with micron spatial resolution in various meteorites. The observed organic-mineral associations may suggest possible origin and formation mechanisms and parent body processes. Three-dimensional (3D) IR microtomography with high spatial resolution has recently become possible.<sup>34</sup> This eliminates ambiguities due to overlapping pixels in the 2D analysis, providing a full mid-IR range spectrum for every voxel in the form of a four-dimensional hyper-data-cube. Indeed, Ebel et al.<sup>35</sup> argued that one should seek evidence of parent body processes from 3D mapping since these processes occur in 3D space.

To our knowledge, no study exists to date on 3D IR microtomography of an astronomical sample. Here we demonstrate this nondestructive analytical technique in a single grain of the Murchison meteorite. This synchrotron-based 3D FT-IR imaging spectro-microtomography has high potential to reveal detailed information on the origin and evolution of materials and processes in extraterrestrial samples, including those to be returned by missions such as Osiris-REx and Hayabusa-2. Here, distribution and relationships between silicates, sulfates, carbonates, water, and aliphatic hydrocarbons are revealed in Murchison.

## Samples and Experimental Details

Fourier transform IR spectro-microtomography was performed at the IRENI (IR ENvironmental Imaging) beamline of the Synchrotron Radiation Center, University of Wisconsin, Madison. Experimental protocols were similar to the acquisition of 2D FT-IR images of meteorites described in Yesiltas et al.,<sup>19,31–33</sup> except that the meteorite sample was rotated to obtain a large number of transmission images. These constitute the tomographic data set.<sup>34</sup>

A single  $\sim 40 \times 50 \mu\text{m}$  pristine Murchison grain was mounted on the tip of a MiTeGen sample holder<sup>34</sup> which was subsequently mounted to the sample rotation stage. Using a 15X (N.A. = 0.5) condenser and a 36X (N.A. = 0.5) objective, the microscope was focused onto the meteorite grain. Precise rotation of the stage under the microscope was computer controlled.<sup>36</sup> The Murchison grain was rotated in increments of  $1.6^\circ$ . At each angle, an IR transmission spectrum was collected for each pixel in a 2D array detector simultaneously. A total of 224 2D transmission images were collected over the  $358.4^\circ$  range of angles.

Each 2D image had the same  $128 \times 128$  pixel field of view, providing  $1.1 \mu\text{m} \times 1.1 \mu\text{m}$  spatial sampling and  $8 \text{cm}^{-1}$  spectral resolution. Thus, the 3D reconstruction of Murchison consists of millions of voxels, each with  $1.1 \mu\text{m} \times 1.1 \mu\text{m} \times 1.1 \mu\text{m}$  volume and a full IR spectrum.

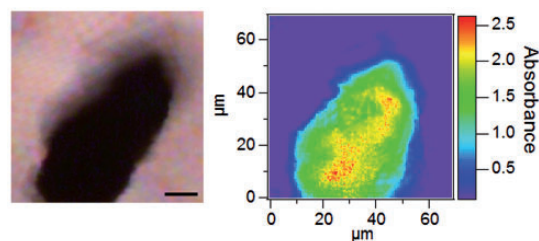
Reconstruction of tomographic data is done in software.<sup>34</sup> Using Igor Pro and IRidys, we first analyzed one of the 224 2D data sets (Figure 1) and identified spectral signatures of molecular functional groups and their corresponding frequency ranges (Figure 2). Subsequently, we used tomography scripts from ImageJ to reconstruct the entire data set and integrated intensity of each characteristic absorbance band. Each reconstruction represents the 3D spatial distribution of a specific functional group within the grain. Finally, generated reconstructions were visualized with Avizo, and different colors were assigned to distinguish them. For purposes of discussing the results, we define a coordinate system such that the vertical coordinate of each voxel is  $x$ , while  $y$  and  $z$  are the two horizontal coordinates.

## Results

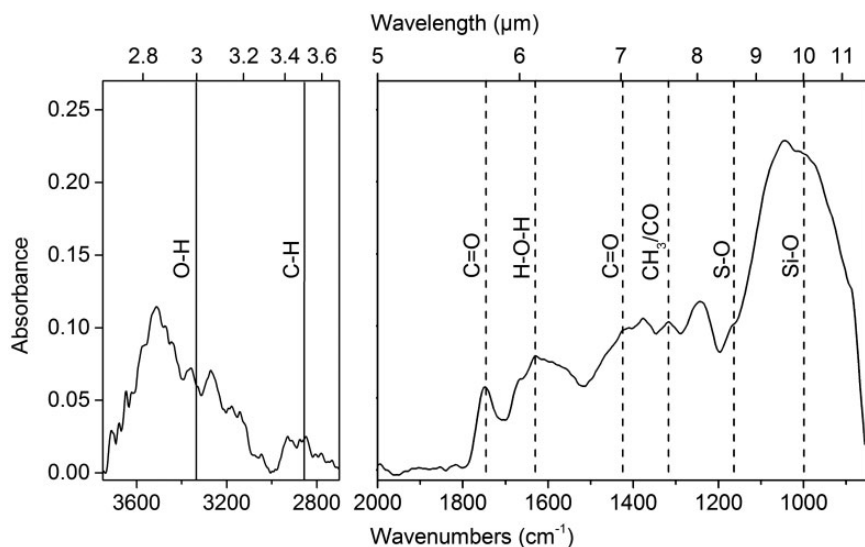
### Identification of Functional Groups

Figure 1 presents both visible (left) and IR (right) micrographs for one of the 2D data sets. The color scale in the IR image represents absorbance, red being the highest. Note that within the spatial resolution defined by the  $3.5 \mu\text{m}$  wavelength, the outlines of the grain in visible and IR images are the same. This indicates that ray deviation caused by index contrast and irregularly orientated surfaces is insignificant on a length scale of  $3.5 \mu\text{m}$ .

Figure 2 presents the grain-averaged IR spectrum of the Murchison grain (after masking the sample-free regions). Distinct absorbance peaks identify the various mineral and molecular functional groups in the studied sample. The clear features are due to silicates, sulfates, aliphatic hydrocarbons, carbonates, water, and carbonyls. Positions and assignments of observed absorbance peaks are collected in Table 1. The spectral region  $2800\text{--}2000 \text{cm}^{-1}$  is omitted due to artifact absorption from atmospheric  $\text{CO}_2$ .



**Figure 1.** Left: visible micrograph of the studied Murchison grain. Horizontal bar is  $\sim 10 \mu\text{m}$ . Right: corresponding IR image of the grain at  $2850 \text{cm}^{-1}$ .



**Figure 2.** Infrared spectrum of the Murchison grain studied in this work. Vertical lines represent positions of specific vibrational modes.

**Table 1.** Integration regions, assignments, and reconstruction labels/colors of functional groups observed in Murchison.

Wavenumber (cm <sup>-1</sup> )	Wavelength (μm)	Vibrational mode	Assignment	Labels/colors in Figure 3
1140–850	8.77–11.76	Si–O stretch	Silicate	a/green
1200–1140	8.33–8.77	S–O stretch	Sulfate	b/yellow
1380–1300	7.19–8.33	CH <sub>3</sub> bend/C–O stretch	Aliphatics	c/pink
1520–1390	6.57–7.19	C=O stretch	Carbonate	d/blue (dark)
1690–1520	5.91–6.57	H–O–H bend	Water	e/red
1790–1690	5.58–5.91	C=O stretch	Carbonyl	f/blue (Cambridge)
3000–2800	3.33–3.57	C–H stretch	Aliphatics	g/blue (light)
3650–3100	2.73–3.22	O–H stretch	Water	h/gray

The broad and well-defined absorbance band near 1000 cm<sup>-1</sup> is due to Si–O stretching vibrational modes of SiO<sub>4</sub> in silicates. Although mostly hydrous, silicate content of Murchison also includes contributions from anhydrous silicates. These are evident from infrared features at 887 and 1050 cm<sup>-1</sup> due to olivine and pyroxene, respectively.

Two bands give evidence for organic molecules and hydrocarbons. C–H stretching modes in hydrocarbons have bands in the 2800–3000 cm<sup>-1</sup> range. Bending modes of CH<sub>3</sub> in aliphatic hydrocarbons, and C–O stretching modes of organic molecules<sup>37</sup> give rise to multiple IR features in the range 1300–1380 cm<sup>-1</sup>. The spatial distributions of C–H stretch and CH<sub>3</sub>/CO need not be the same.

Two bands give evidence for water. The first is a relatively narrow band near 1630 cm<sup>-1</sup> due to the H–O–H bending mode, which has been interpreted as due to interlayer water indigenous to phyllosilicates.<sup>38</sup> The second is a broad band in the range 3700–3000 cm<sup>-1</sup> due to the O–H stretch. Interlayer water in phyllosilicates certainly contributes to this band, but there also may be contributions from

carboxyls and alcohols. Water may also be present as an adsorbed terrestrial contaminant.<sup>39</sup>

Asymmetric stretching vibrations of C=O in the carbonate CO<sub>3</sub><sup>2-</sup> ion are responsible for the band near 1427 cm<sup>-1</sup>. The feature near 1160 cm<sup>-1</sup> is probably due to S–O stretching modes in sulfates, consistent with the known presence of sulfates in Murchison.<sup>40</sup> The strong and distinct absorbance band near 1740 cm<sup>-1</sup> is due to C=O stretching modes in carbonyls, such as ketone, also previously identified in Murchison.<sup>41,42</sup>

### Three-Dimensional Reconstructions

Based on spectral positions of absorbance bands and their respective assignments presented in the previous section, we generated 3D reconstructions of individual molecular functional groups. Concentrations are defined as regions where that group's absorbance exceeds its grain average. Figure 3 presents selected 2D projections of these reconstructions. See the online Supplemental Material for video rotations.

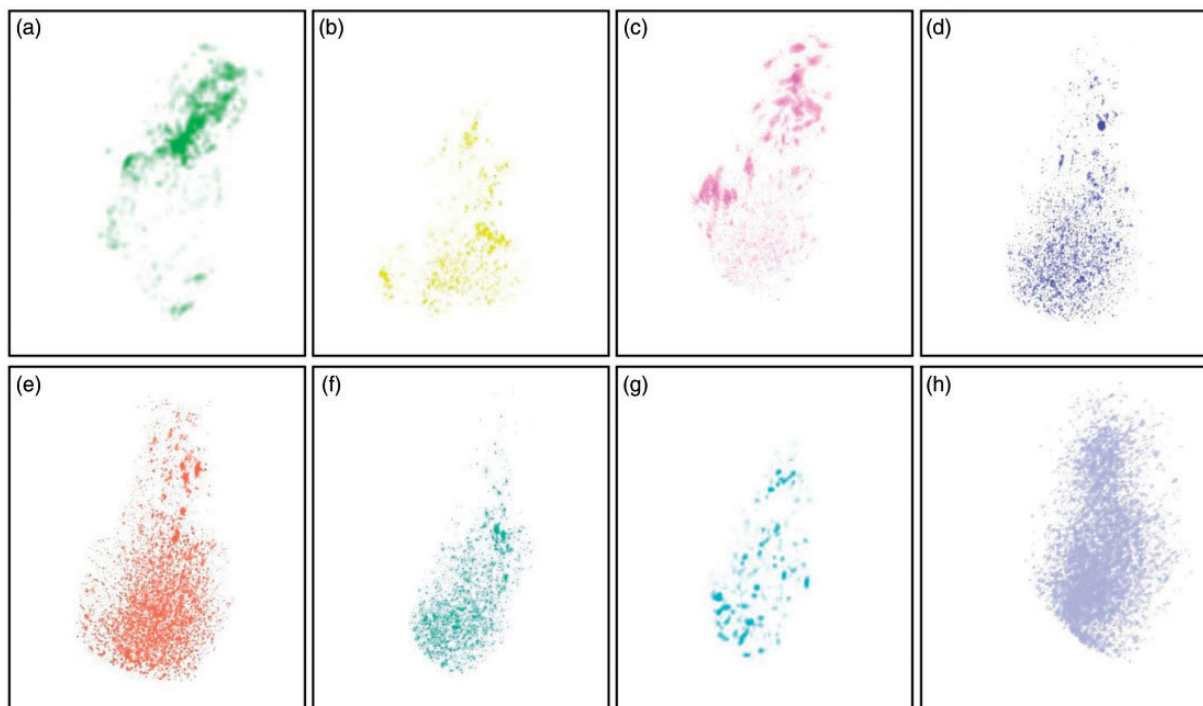


**Figure 3.** Images of 3D reconstructions of organics and minerals. (a) Si–O stretch in silicates, (b) S–O stretch in sulfates, (c) C–H bend / C–O stretch, (d) C=O stretch in carbonates, (e) O–H bend in water, (f) C=O stretch in carbonyls, (g) C–H stretch in aliphatics, (h) O–H stretch in water.

The upper half of the grain is relatively rich in silicates (Figure 3a). The connected regions with higher than average silicate concentration are significantly larger in the upper half of the grain than in the lower half. Close inspection shows that none of the connected regions of higher silicate concentration has a dimension exceeding about  $8\ \mu\text{m}$ , i.e., they are all smaller than the wavelength of the silicate band. (Although the spatial resolution is of course no better than the wavelength, there are variations nevertheless in the strength of every band on sub-wavelength length scales.)

Sulfate-rich material occurs as a dense constellation of small blobs located along part of the surface on the lower half of the grain (Figure 3b). There are a few larger blobs of higher than average sulfate concentration in the upper half of the grain. The video rotations make clear that the spatial distribution of sulfate concentrations is well separated from that of the silicate concentrations.

Aliphatic hydrocarbon concentrations based on  $\text{CH}_3$  bends (Figure 3c) appear as coarse blobs, mainly in the upper half of the grain. Several of these about halfway down the grain appear in the video rotations as very thin ( $<2\ \mu\text{m}$ ) platelets of up to  $6\ \mu\text{m}$  diameter and aligned with the surface like layers of an onion. The coincidence of silicate and  $\text{CH}_3/\text{CO}$  concentrations in the upper half of the grain, may suggest that synthesis of certain organic molecules are catalyzed by phyllosilicates, either in the parent body or in the interstellar medium (ISM).

C–H stretch concentrations (Figure 3g) appear as small blobs with higher abundance in the lower half of the grain. The video rotations support that they are spatially distinct from the  $\text{CH}_3/\text{CO}$  concentrations (Figure 3c). Notably, the C–H stretch blobs halfway down the grain appear on the opposite side of the grain from the thin platelets of high  $\text{CH}_3/\text{CO}$  concentration. Thus, there appear to be distinct populations of organic molecules, with the  $\text{CH}_3/\text{CO}$  concentrations possibly weighted toward the C–O stretch. Considering the observations made in the preceding paragraph, it may be mainly those organics that contain oxygen that are catalyzed by phyllosilicates. Perhaps it is interaction with the water in phyllosilicates which oxidizes the carbon in carbonaceous meteorites.

Concentrations of water obtained from H–O–H bends are distributed roughly uniformly throughout the grain as small blobs (Figure 3e). Concentrations of O–H stretches are also located throughout the sample (Figure 3h), but their distribution differs from that for the H–O–H bend. That means that some of the O–H stretch in Murchison is due molecules other than water, such as alcohols and carboxyls. Substantial presence of hydrated silicates (phyllosilicates) in Murchison is evident from the partial overlap in the spatial distributions of silicate and O–H concentrations.

Carbonate concentrations from the C=O stretch (Figure 3d) are distributed throughout the grain similarly to the H–O–H bend of water (Figure 3e). They do not

perfectly coincide, but they appear to be positively correlated.

The carbonyl concentrations are distinct from the others, appearing mostly in the lower half of the grain (Figure 3f). Notably, high concentrations of carbonyl are separate from high concentrations of silicates and  $\text{CH}_3/\text{CO}$ .

In addition to the reconstructions of individual concentrations, we consider pair-wise comparisons. Figure 4a shows that concentrations of silicates and O–H stretch overlap in the upper half of the grain but much less so in the lower half due to lack of silicates there. In the upper half, some silicate-rich blobs appear to be spatially distinct from the O–H stretch, indicating separated concentrations of hydrous and anhydrous silicates.

Concentrations of C–H stretch appear spatially distinct from those of silicates (Figure 4b), overlapping only a little near the upper regions. This means that a significant population of hydrocarbons is unlikely to have origins associated with phyllosilicates.

Figure 4c shows that C–H stretch concentrations have considerable overlap with those of carbonates. This is perhaps due to the accidental coincidence between the overtones of carbonates<sup>43</sup> and the C–H stretch absorption.

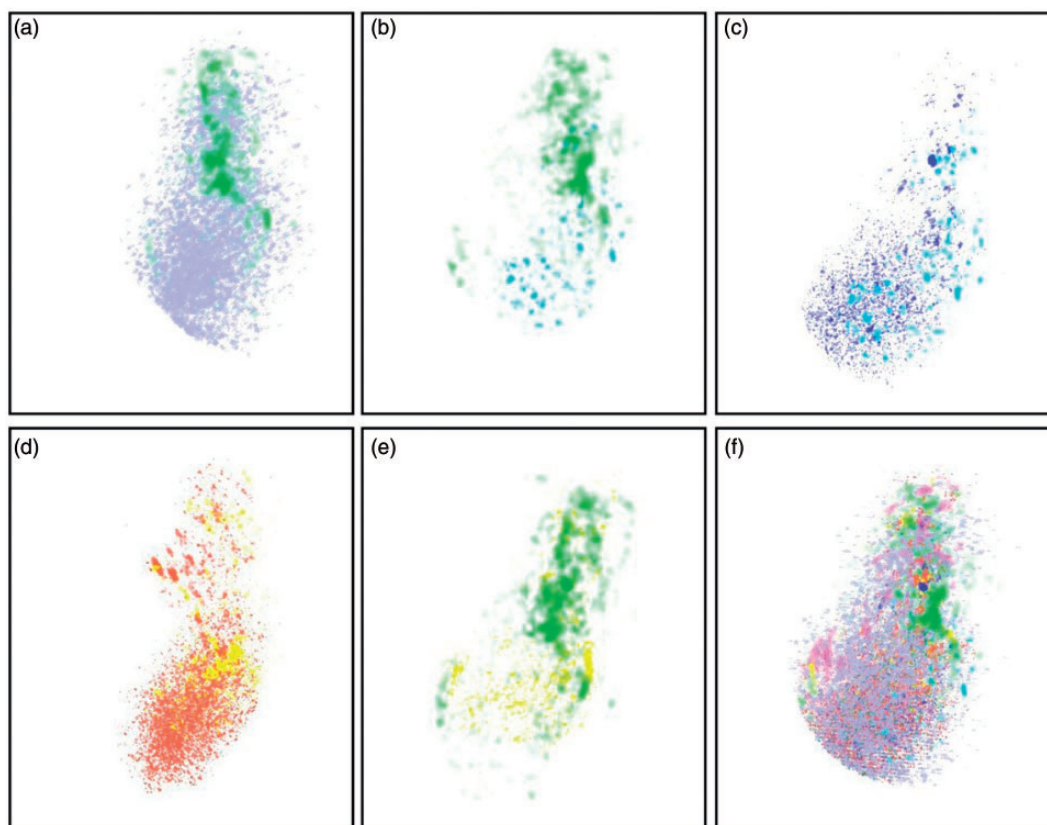
Sulfate and H–O–H bend concentrations appear to overlap well. Sulfate concentrations are contained mostly within the relatively wet region (Figure 4d). This may have implications regarding the formation of sulfates from aqueous alteration.

Figure 4e shows relative spatial distributions for concentrations of sulfates and silicates. This image, together with the 3D video rotations, confirm that sulfate and silicate concentrations are spatially separated, as has already been noted.

Finally, we generated a superposition of reconstructions for all of the components in Figure 4f. Note the empty regions especially around the edges of the grain. These are voxels for which the absorbance of every group is below the grain average. The optical path through these edge regions might be less than the  $\sim 1 \mu\text{m}$  spatial resolution, i.e., these voxels are incompletely filled with matter.

#### Two-Dimensional Versus Three-Dimensional Correlation Analysis

We have previously published correlation analysis between different mineral groups and organics for grains of the



**Figure 4.** Images of combined 3D reconstructions of organics and minerals.



meteorites Sutter's Mill<sup>19</sup> and NWA 852.<sup>32</sup> An acknowledged uncertainty in those studies is the possibility of accidental coincidences due to the integration of absorption from material in a column of voxels that passes from one side of the grain to the other. In other words, the absorption of one mineral near the top surface can be superimposed on the absorption of material from near the bottom surface along a given ray of the transmitted IR beam, giving a false spatial correlation. We argued in those papers that by looking at a large number of pixels from the 2D spectral image with high spatial resolution, the impact of such accidental correlations is averaged out. However, to emphasize the advantage of 3D tomography, we present an example for the presently studied meteorite grain, which shows that 2D correlation analysis from too few pixels can give results that differ from conclusions of the 3D investigation. To do this, we extracted IR spectra from vertical columns of voxels ( $x$ -axis) for fixed  $z = 64$  and  $y = 15, 30, 45, 60, 75, 90,$  or  $105$ . For each column, sample-free voxels were excluded and the remaining voxels were averaged. Figure 5 presents these spectra. Vertical lines indicate IR features of specific functional groups, as in Figure 2.

We performed correlation analyses based on integrated intensity of the Gaussian-fit bands for the seven columns sampled. Figure 6 presents the results with correlation coefficient ( $r$ ) at a 95% confidence level. Sulfates are positively correlated with carbonates, which is compatible with the observation from Figures 3 and 4 that both are correlated with H–O–H bend (and hence with each other). On the other hand, the correlation in Figure 6 between silicates and carbonates implies that silicates and sulfates must also be correlated, which contradicts our earlier conclusion. Moreover, the 2D analysis misses some conclusions previously made from the 3D analysis. These observations emphasize the uncertainties inherent to correlation analysis based on limited sampling of pixels from 2D spectral imaging, and they emphasize the advantage of the 3D approach presented here.

## Discussion

Spatial correlation between organic molecules and minerals in primitive meteorites can provide insights on the origin and evolution of organic matter. Formation regions, conditions, and pathways of organic molecules found in meteorites can vary. For instance, they can form in the solar nebula via ultraviolet irradiation of icy grains,<sup>44</sup> or in the ISM via grain surface-gas phase reactions,<sup>11</sup> or through catalytic reactions on grain surfaces in the parent body.<sup>12</sup>

Most investigations of organic matter in meteorites have chemically extracted the organics by demineralizing the inorganic content.<sup>45–48</sup> This method loses mineralogical context, may possibly alter organic matter by the acids used,<sup>49</sup> and misses some of the organic matter.<sup>50</sup> In contrast, our technique maps organic and mineral composition

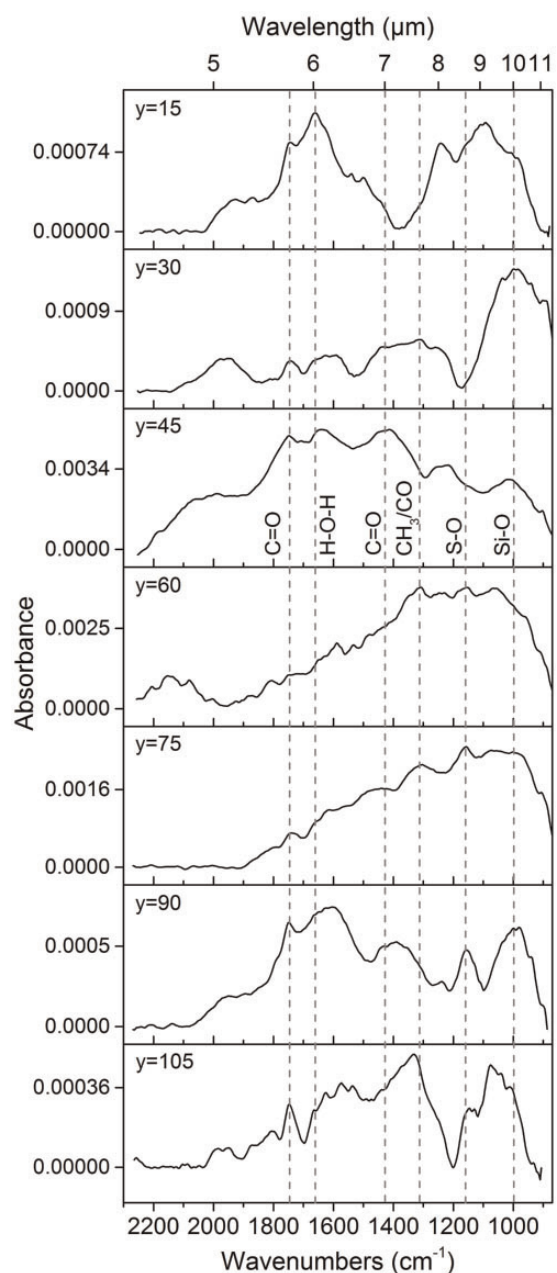


**Figure 5.** Infrared spectra of rows on the  $x$ -axis, extracted from different  $y$ -axes for  $z = 64$ . Vertical dashed lines show position of different functional groups.

of Murchison meteorite in situ without chemical treatment, and it allows us to study organic-mineral associations at micron length scales.

Supporting the observation of variety and segregation for different types of organics, Murchison is already known to be one of the most heterogeneous meteorites, containing a broad spectrum of organics. Cronin and Pizzarello<sup>50</sup> found that principal components within the aliphatics of the Murchison are alkanes including cyclic alkanes, which means that some aliphatic hydrocarbons

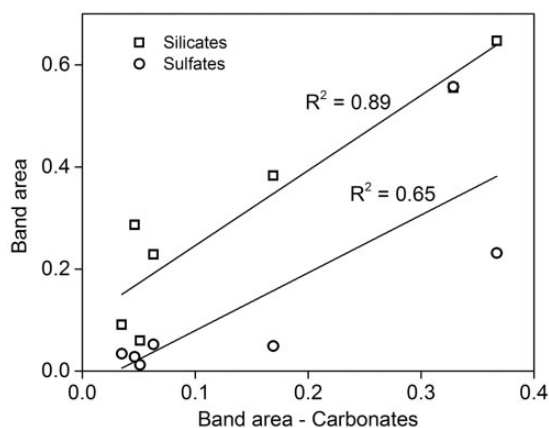


**Figure 6.** Variations of band areas of silicates and sulfates relative to that of carbonates. Straight lines indicate linear fits with corresponding  $r$  values obtained with 95% confidence level.

contain rings of  $\text{CH}_3$ . Also, they found that hydrocarbons were highly branched, which means there are more  $\text{CH}_3$  moieties attached to the aliphatic chains. We found absorbance band ratio of  $\text{CH}_2/\text{CH}_3$  to be around 1, so there is no significant preference of  $\text{CH}_2$  over  $\text{CH}_3$ , which is consistent with aliphatics being highly branched.

On the basis of the remarkably similar IR spectra of Murchison and ISM in the  $2800\text{--}3000\text{ cm}^{-1}$  region, it has been suggested<sup>51</sup> that some ISM components may have survived to be incorporated into the meteorite parent body in the case of Murchison. We measured a series of Murchison grains in the mid-IR and obtained the  $\text{CH}_2/\text{CH}_3$  ratio to be 1.10, which is comparable to the published data for Murchison (1.00)<sup>18</sup> as well as ISM ( $\sim 1.10$ ).<sup>52,53</sup> Such a small ratio points to short and/or highly branched aliphatic chains, whose formation regions and conditions were perhaps similar to those in the ISM.

Though the organic matter in Murchison is spectrally similar to organics in ISM, there is strong possibility that it was later processed by aqueous alteration in the parent body to form a higher quantity and variety of organics. It is usually held that organics are first formed in the ISM and are then transported to the solar nebula, or to a parent body, or sequentially to solar nebula then parent body. In the case of Murchison, it is believed that organics were formed in the ISM, but the highly heterogeneous composition suggests formation of some organics in the parent body through processes such as aqueous alteration, etc. The broad and symmetric absorbance band near  $10\text{ }\mu\text{m}$  wavelength in our spectra is indicative of the presence of phyllosilicates, which must have formed due to aqueous alteration in the parent body. Phyllosilicates also facilitate the formation of organics and sometimes they protect organics from being destroyed or oxidized, which further supports the likelihood that some organics were formed in Murchison's parent body.

Very few previous investigations exist regarding organic-mineral associations in meteorites. Pearson et al.<sup>2</sup> combined osmium labeling, X-ray spectroscopy, and scanning electron microscopy to show that phyllosilicates are associated with organic matter of unknown composition in carbonaceous chondrites, including Murchison. Micro-Raman imaging by Amri et al.<sup>54</sup> showed that pyroxene and carbonaceous matter spatially overlap in Murchison, indicating positive correlation of silicates and organics. Guillou et al.<sup>55</sup> utilized secondary ion mass spectroscopy (SIMS), focused ion beam (FIB), and scanning transmission X-ray microscopy (STXM) to show that diffuse and granular organic matter is intimately mixed (intercalated) with phyllosilicates in Murchison, suggesting an association of organic matter with phyllosilicates and carbonates. Our IR spectroscopic observations of spatial concentrations of various groups and organic-mineral associations in Murchison are in good agreement with these earlier studies by different techniques.<sup>2,49,54</sup>

Next we consider the possibility that optical artifacts affect the accuracy of our results. Scattering, diffraction, and refraction might occur if there were domains larger than the wavelength with significantly different indices. Indeed, Figure 3 might be misinterpreted as evidence of such domains comprising a single pure constituent, e.g., low index organics or high index silicates. However, there is no region larger than our  $1.1\text{ }\mu\text{m}$  spatial sampling that is pure anything. Silicates and organics are distributed continuously (though with varying concentration) throughout the grain. Figure 3 comprises binary representations of a continuous concentration distribution, like a black and white print with no gray scale, so that, for example, a silicate blob is not a hard-edged silicate rock. The boundaries of the regions in Figure 3 merely indicate where the absorbance crosses a threshold value, defined as the grain-averaged absorbance for that mineral group. Silicate absorbance is found in the spectrum of every voxel. This applies also to the 2D pixels in the images of other meteorite grains as well, e.g., to Sutters Mill,<sup>19</sup> NWA 852,<sup>32</sup> Tagish Lake.<sup>33</sup> X-ray fluorescence (XRF) with  $1\text{ }\mu\text{m}$  spatial resolution (Juergen Thieme, SRX beamline, NSLS-II, Brookhaven National Laboratory, private communication) on a set of grains from the same Murchison sample confirms the continuity of the silicate distribution. Results confirm that there is no region on the surface of any grain that is free of silicon. The Si XRF signal, though heterogeneous, never vanishes on the surface of any grain and all Si XRF intensities significantly exceeded the detection limit.

Not only is the grain free internally from strong index contrasts, but also the length scales for the index variations that exist are all sub-wavelength. Although Figure 3a shows a stringy blob stretched diagonally across the upper half of the grain by more than  $20\text{ }\mu\text{m}$ , this is an artifact of viewing only a single image from the 3D reconstruction at relatively low spatial resolution and contrast. In fact, no blob of

silicate-rich material is larger than  $\sim 8 \mu\text{m}$ . We suspect that the true characteristic length scale for index variations is sub-micron, though our technique cannot show it.

In ray optics, we must average over length scales much larger than the wavelength.<sup>56</sup> The longest dimension of our grain is only  $15 \times$  our smallest wavelength. Thus, the IR radiation propagating through our meteorite grain is passing through an effectively homogenous medium described by effective optical constants. Scattering, diffraction, and refraction caused by sub-wavelength and low-contrast internal index variations should be absent. Were the variations present, they would create the signature artifacts described in the online version and Supplemental Material of Martin et al.,<sup>34</sup> using the same apparatus and 3D reconstruction software that we used here. A hard-edged, high-index structure several times larger than the wavelength can diffract light to cause intensity oscillations in the image, but only if the wavelength is not strongly absorbed by the structure. These oscillations are particularly apparent in the geometrical shadow of the structure, causing the structures to appear hollow and sharpening their edges. We observe no such intensity oscillations, no hollow concentrations, and no sharp edges. The high absorption that defines mineral concentrations additionally explains why such signature artifacts are absent.

Strongly scattered rays are not collected by the spectrometer or imaging optics. The well-known spectral signature of such scattering is a rapid intensity decrease with increasing wavenumber,<sup>57</sup> but no such effect is observed in our spectra. Moderately scattered rays (other than by diffraction) that happened to be collected and imaged onto the detector array would contribute mainly a contrast-lowering haze (as known for cataracts of the eye). Large and moderate angle scattering cannot artificially produce well-defined regions of stronger absorption where none exist.

One might object that the index contrast between the air and our meteorite grain is not small, so that refraction at the grain boundaries could be significant. Indeed, our absorption data suggest that the edges of the sample present less of an optical path length than the center. In other words, each grain might act like a lens, giving very strong distortion of the 2D image. However, the observations do not support such a negative situation for our meteorite grains, presumably because of the small optical paths in the optically dense medium where all dimensions are not much larger than the wavelength. Our optical microscope and IR images for hundreds of different meteorite grains show that grain outline at visible wavelengths is always well preserved in the IR within the resolution limits, so that image distortion is insignificant. Figure 1 is an example for the grain considered in this paper. Yesiltas et al.<sup>19,33</sup> present other examples.

There have been many completely independent demonstrations of IR tomography where the same concerns regarding index gradients apply. For long optical paths with strong

scattering, as in near-IR medical imaging, the Radon transform (which assumes undeflected beams) does not apply, and different reconstructions are used.<sup>58,59</sup> In the far-IR (THz), where scattering is weaker, the main effect of index contrast is a loss of collected signal due to strong refraction at the air-sample interface.<sup>59,60</sup> It can then be difficult to discriminate whether the image contrast is due to absorption or beam deviation. However, in our experiment, we do determine that the contrast arises from absorption, and not deviation, because for each pixel we have a broadband mid-IR spectrum, and attenuation of light is associated with a characteristic absorption band which can be unambiguously associated with a specific mineral or molecular group.

Very recently, Quaroni et al.<sup>61</sup> demonstrated 3D mid-IR tomographic imaging of endogenous and exogenous molecules in a single intact cell with subcellular resolution using instrumentation that is very similar to ours. In their work, they demonstrated the experimental method as well as the quantitative 3D distribution of molecular components based on the intrinsic contrast provided by their sample. In their report, they stated that “the introduction of cellular IR tomography will be one of the breakthroughs that will revolutionize IR imaging of biological systems,” and that “the applicability of the technique is general and not limited to plant cells, the same protocols described in this work can be used for benchtop tomographic imaging of any cells and any other samples accessible by an IR transmission measurement.”<sup>61</sup>

According to Guillet et al.,<sup>62</sup> IR transmission images may be used for tomography by the same procedures used to acquire and to render 3D images in the optical, IR, or X-ray regions of the electromagnetic spectrum. Many experimental reports have demonstrated the successful application of those procedures. In several cases where the structure is known in advance, so that the spatial index variations are known, and where the index contrast is strong and the surfaces convoluted, IR tomography has confirmed the structure without distortion.<sup>60,62–66</sup> This gives confidence to the application of the technique to situations such as ours, where the structure and index distribution is unknown in advance, though the index variations are expected from complementary measurements to be small.

## Conclusion

We presented the first ever 3D spectro-microtomography measurement on an extraterrestrial sample in situ in the IR with high spatial resolution. This nondestructive technique reveals spatial relationships between organics and minerals, elucidating their origins and processing. These spectral data can be quantitatively interpreted using principle component and correlation analyses. The technique has significant potential for the in situ investigation of extraterrestrial samples, including those returned from missions such as Osiris-Rex and Hayabusa-2 to primitive asteroids.



The highly heterogeneous chemical composition of Murchison contains signatures of processes that took place in the ISM as well as in the parent body, both of which contributed to the synthesis of organic molecules. For the considered Murchison grain, the spatial distribution relative to water identifies hydrous and anhydrous silicates. Sulfates are found to be surrounded by water. Proximity of phyllosilicates to CH<sub>3</sub> and CO suggests a role for hydrated silicates in the formation of certain organics. The CH<sub>2</sub>/CH<sub>3</sub> ratio is as small as that of ISM (~1.00), suggesting the same formation regions and/or conditions for their organic matter.

### Acknowledgments

The authors thank Prof. Daniel Britt for providing the Murchison sample and Prof. Timothy Glotch for constructive comments. They also give special thanks to Juergen Thieme and his research group at the Brookhaven National Laboratory for performing X-ray fluorescence spectroscopy. The authors would also like to acknowledge support for IRENI from the US Forest Products Laboratory in Madison.

### Conflict of Interest

The authors report there are no conflicts of interest.

### Funding

Mehmet Yesiltas is primarily supported through graduate fellowship Program #1416 by the Turkish government. SRC is primarily funded by the University of Wisconsin–Madison with supplemental support from facility users and the University of Wisconsin–Milwaukee. The beamline construction and development of IRENI was supported by NSF MRI award # 0619759. CJH is funded by NSF CHE award # 1112433.

### Supplemental Material

All supplemental material mentioned in the text, consisting of 14 videos, is available in the online version of the journal.

### References

1. P. Beck, A. Garenne, E. Quirico, L. Bonal, G. Montes-Hernandez. "Transmission Infrared Spectra (2–25 Microns) of Carbonaceous Chondrites (CI, CM, CV-CK, CR, C2 Ungrouped): Mineralogy, Water, and Asteroidal Processes". *Icarus*. 2014. 229: 263–277.
2. V.K. Pearson, M.A. Sephton, A.T. Kearsley, P.A. Bland, I.A. Franchi, I. Gilmour. "Clay Mineral–Organic Matter Relationships in the Early Solar System". *Meteoritics Planetary Sci.* 2002. 37(12): 1829–1833.
3. J. Lederberg, D.B. Cowie. "Moon dust: The Study of this Covering Layer by Space Vehicles May Offer Clues to the Biochemical Origin of Life". *Science*. 1958. 127(3313): 1473–1475.
4. R. Hayatsu, M.H. Studier, E. Anders. "Origin of Organic Matter in Early Solar System—IV. Amino Acids: Confirmation of Catalytic Synthesis by Mass Spectrometry". *Geochim. Cosmochim. Acta*. 1971. 35(9): 939–951.
5. E. Anders, R. Hayatsu, M.H. Studier. "Interstellar Molecules: Origin by Catalytic Reactions on Grain Surfaces". *Astrophys. J.* 1974. 192: L101–L105.
6. R. Hayatsu, E. Anders. "Organic Compounds in Meteorites and their Origins". *Cosmo- and Geochemistry*. 1981. 99: 1–37.
7. C. Ponnampertuma, A. Shimoyama, E. Friebele. "Clay and the Origin of Life". *Orig. Life*. 1982. 12(1): 9–40.
8. C. Chyba, C. Sagan. "Endogenous Production, Exogenous Delivery and Impact-Shock Synthesis of Organic Molecules—An Inventory for the Origins of Life". *Nature*. 1992. 355: 125–132.
9. R. Saladino, C. Crestini, G. Costanzo, R. Negri, E. Di Mauro. "A Possible Prebiotic Synthesis of Purine, Adenine, Cytosine, and 4(3H)-Pyrimidinone from Formamide: Implications for the Origin of Life". *Bioorg. Med. Chem.* 2001. 9(5): 1249–1253.
10. P. Ehrenfreund, W. Irvine, L. Becker, J. Blank, J.R. Brucato, L. Colangeli, S. Derenne, D. Despois, A. Dutrey, H. Fraaije, A. Lazcano, T. Owen, F. Robert, International Space Science Institute Issi Team. "Astrophysical and Astrochemical Insights into the Origin of Life". *Rep. Progr. Phys.* 2002. 65(10): 1427–1487.
11. P. Ehrenfreund, S.B. Charnley. "Organic Molecules in the Interstellar Medium, Comets, and Meteorites: A Voyage from Dark Clouds to the Early Earth". *Annu. Rev. Astron. Astrophys.* 2000. 38(1): 427–483.
12. S. Pizzarello, E. Shock. "The Organic Composition of Carbonaceous Meteorites: The Evolutionary Story Ahead of Biochemistry". *Cold Spring Harb. Perspect. Biol.* 2010. 2(3): a002105.
13. J.H. Cleaves, S.A. Michalkova, F.C. Hill, J. Leszczynski, N. Sahai, R. Hazen. "Mineral–Organic Interfacial Processes: Potential Roles in the Origins of Life". *Chem. Soc. Rev.* 2012. 41: 5502–5525.
14. E. Cloutis, P. Hudon, T. Hiroi, M. Gaffey. "Spectral Reflectance Properties of Carbonaceous Chondrites: 3. CR Chondrites". *Icarus*. 2012. 217(1): 389–407.
15. V. Pearson, M. Sephton, I. Franchi, J. Gibson, I. Gilmour. "Carbon and Nitrogen in Carbonaceous Chondrites: Elemental Abundances and Stable Isotopic Compositions". *Meteoritics Planetary Sci.* 2006. 41(12): 1899–1918.
16. C.D.K. Herd, A. Blinova, D.N. Simkus, Y. Huang, R. Tarozo, C.M.O.D. Alexander, F. Gyngard, L.R. Nittler, G.D. Cody, M.L. Fogel, Y. Kebukawa, A.L.D. Kilcoyne, R.W. Hilts, G.F. Slater, D.P. Glavin, J.P. Dworkin, M.P. Callahan, J.E. Elsila, B.T. De Gregorio, R.M. Stroud. "Origin and Evolution of Prebiotic Organic Matter as Inferred from the Tagish Lake Meteorite". *Science*. 2011. 332(6035): 1304–1307.
17. S. Merouane, Z. Djouadi, L. Le. Sergeant d'Hendecourt. "Relations between Aliphatics and Silicate Components in 12 Stratospheric Particles Deduced from Vibrational Spectroscopy". *Astrophys. J.* 2014. 780(2): 174–186.
18. Y. Kebukawa, S. Nakashima, M. Ishikawa, K. Aizawa, T. Inoue, K. Nakamura-Messenger, M.E. Zolensky. "Spatial Distribution of Organic Matter in the Bells CM2 Chondrite Using Near-Field Infrared Microspectroscopy". *Meteoritics Planetary Sci.* 2010. 45(3): 394–405.
19. M. Yesiltas, Y. Kebukawa, R.E. Peale, E. Mattson, C.J. Hirschmugl, P. Jenniskens. "Infrared Imaging Spectroscopy with Micron Resolution of Sutter's Mill Meteorite Grains". *Meteoritics Planetary Sci.* 2014. 49(11): 2027–2037.
20. E. Palomba, A. Rotundi, L. Colangeli. "Infrared Micro-Spectroscopy of the Martian Meteorite Zagami: Extraction of Individual Mineral Phase Spectra". *Icarus*. 2006. 182(1): 68–79.
21. S.A. Sandford, S.N. Milam, M. Nuevo, P. Jenniskens, M.H. Shaddad. "The Mid-Infrared Transmission Spectra of Multiple Stones from the Almahata Sitta Meteorite". *Meteoritics Planetary Sci.* 2010. 45(10–11): 1821–1835.
22. A. Wang, K. Kuebler, B. Jolliff, L.A. Haskin. "Mineralogy of a Martian meteorite as Determined by Raman Spectroscopy". *J. Raman Spectrosc.* 2004. 35(6): 504–514.
23. H. Busemann, C.M.O.D. Alexander, L.R. Nittler. "Characterization of Insoluble Organic Matter in Primitive Meteorites by MicroRaman Spectroscopy". *Meteoritics Planetary Sci.* 2007. 42(7–8): 1387–1416.

24. J.N. Grossman, A.J. Brearley. "The Onset of Metamorphism in Ordinary and Carbonaceous Chondrites". *Meteoritics Planetary Sci.* 2005. 40: 87–122.
25. R.M. Izawa, R.L. Flemming, P.L. King, R.C. Peterson, P.J.A. McCausland. "Mineralogical and Spectroscopic Investigation of the Tagish Lake Carbonaceous Chondrite by X-ray Diffraction and Infrared Reflectance Spectroscopy". *Meteoritics Planetary Sci.* 2010. 45(4): 675–698.
26. O. Menzies, P. Bland, F. Berry, G. Cressey. "A Mössbauer Spectroscopy and X-ray Diffraction Study of Ordinary Chondrites: Quantification of Modal Mineralogy and Implications for Redox Conditions During Metamorphism". *Meteoritics Planetary Sci.* 2005. 40(7): 1023–1042.
27. G. Flynn, L. Keller, C. Jacobsen, S. Wirick. "An Assessment of the Amount and Types of Organic Matter Contributed to the Earth by Interplanetary Dust". *Adv. Space Res.* 2004. 33(1): 57–66.
28. Y. Kebukawa, M.E. Zolensky, A.L.D. Kilcoyne, Z. Rahman, P. Jenniskens, T. Mikouchi, K. Hagiya, K. Ohsumi, M. Komatsu, G.D. Cody. "Organic Analysis of Sutter's Mill Chondrite Using C-XANES". *Lunar and Planetary Science Conference Abstract #2118*. 2013.
29. S.A. Sandford, J. Aléon, C.M.O.D. Alexander, T. Araki, S. Bajt, G.A. Baratta, J. Borg, J.P. Bradley, D.E. Brownlee, J.R. Brucato. "Organics Captured from Comet 81P/Wild 2 by the Stardust Spacecraft". *Science*. 2006. 314(5806): 1720–1724.
30. A. Morlok, C. Koike, K. Tomeoka, A. Mason, C. Lisse, M. Anand, M. Grady. "Mid-Infrared Spectra of Differentiated Meteorites (Achondrites): Comparison with Astronomical Observations of Dust in Protoplanetary and Debris Disks". *Icarus*. 2012. 219(1): 48–56.
31. M. Yesiltas, C.J. Hirschmugl, R.E. Peale. "In Situ Investigation of Meteoritic Organic-Mineral Relationships by High Spatial Resolution Infrared Spectroscopy". *Meteoritics Planetary Sci.* 2013. 48: S5.
32. M. Yesiltas, R.E. Peale, M. Unger, J. Sedlmair, C.J. Hirschmugl. "Organic and Inorganic Correlations for Northwest Africa 852 by Synchrotron-Based Fourier Transform Infrared Microspectroscopy". *Meteoritics Planetary Sci.* 2015. 50: 1684–1696.
33. M. Yesiltas, Y. Kebukawa. "Associations of Organic Matter with Minerals in Tagish Lake Meteorite via High Spatial Resolution Synchrotron-Based FT-IR Microspectroscopy". *Meteoritics Planetary Sci.* 2016. 51(3): 584–595.
34. M.C. Martin, C. Dabat-Blondeau, M. Unger, J. Sedlmair, D.Y. Parkinson, H.A. Bechtel, B. Illman, J.M. Castro, M. Keiluweit, D. Buschke, B. Ogle, M.J. Nasse, C.J. Hirschmugl. "3D Spectral Imaging with Synchrotron Fourier Transform Infrared Spectro-Microtomography". *Nat. Meth.* 2013. 10: 861–864.
35. D.S. Ebel, M.L. Rivers. "Meteorite 3-D Synchrotron Microtomography: Methods and Applications". *Meteoritics Planetary Sci.* 2007. 42(9): 1627–1646.
36. E.C. Mattson, M. Unger, J. Sedlmair, M. Nasse, E. Aboualizadeh, Z. Alavi, C.J. Hirschmugl. "Widefield FT-IR 2D and 3D Imaging at the Microscale Using Synchrotron Radiation". In: R. Salzer, H.W. Siesler (eds) *Infrared and Raman Spectroscopic Imaging: Second, Completely Revised and Updated Edition*. Weinheim, Germany: Wiley-VCH Verlag GmbH & Co, 2014, pp.263–277.
37. B.H. Stuart. "Infrared Spectroscopy: Fundamentals and Applications". In: D.J. Ando (ed.) *New York, USA: John Wiley & Sons, Ltd*, 2004.
38. G. Matrajt, G.M. Muñoz Caro, E. Dartois, L. D'Hendecourt, D. Deboffe, J. Borg. "FT-IR Analysis of the Organics in IDPs: Comparison with the IR Spectra of the Diffuse Interstellar Medium". *Astron. Astrophys.* 2005. 433: 979–995.
39. C. Che, T.D. Glotch, D.L. Bish, J.R. Michalski, W. Xu. "Spectroscopic Study of the Dehydration and/or Dehydroxylation of Phyllosilicate and Zeolite Minerals". *J. Geophys. Res.* 2011. 116: E05007.
40. S.A. Airieau, J. Farquhar, M.H. Thiemens, L.A. Leshin, H. Bao, E. Young. "Planetary Sulfate and Aqueous Alteration in CM and CI Carbonaceous Chondrites". *Geochim. Cosmochim. Acta.* 2005. 69(16): 4167–4172.
41. G.A. Jungclaus, G.U. Yuen, C.B. Moore, J.G. Lawless. "Evidence for the Presence of Low Molecular Weight Alcohols and Carbonyl Compounds in the Murchison Meteorite". *Meteoritics*. 1976. 11: 231–237.
42. F.R. Orthous-Daunay, E. Quirico, P. Beck, O. Brissaud, E. Dartois, T. Pino, B. Schmitt. "Mid-Infrared Study of the Molecular Structure Variability of Insoluble Organic Matter from Primitive Chondrites". *Icarus*. 2013. 223(1): 534–543.
43. M. Nuevo, S.A. Sandford, G.J. Flynn, S. Wirick. "Mid-IR Study of Stones from the Sutter's Mill Meteorite". *Meteoritics Planetary Sci.* 2014. 49(11): 2017–2026.
44. F.J. Ciesla, S.A. Sandford. "Organic Synthesis via Irradiation and Warming of Ice Grains in the Solar Nebula". *Science*. 2012. 336: 452–454.
45. E. Quirico, F.R. Orthous-Daunay, P. Beck, L. Bonal, R. Brunetto, E. Dartois, T. Pino, G. Montagnac, J.N. Rouzaud, C. Engrand, J. Duprat. "Origin of Insoluble Organic Matter in Type I and 2 Chondrites: New Clues, New Questions". *Geochim. Cosmochim. Acta.* 2014. 136: 80–99.
46. G. Briani, E. Quirico, M. Gounelle, M. Paulhiac-Pison, G. Montagnac, P. Beck, F.R. Orthous-Daunay, L. Bonal, E. Jacquet, A. Kearsley, S.S. Russell. "Short Duration Thermal Metamorphism in CR Chondrites". *Geochim. Cosmochim. Acta.* 2013. 122: 267–279.
47. S. Pizzarello, G.W. Cooper, G.J. Flynn, D.S. Lauretta, H.Y. McSween. "The Nature and Distribution of the Organic Material in Carbonaceous Chondrites and Interplanetary Dust Particles". In: D.S. Lauretta, H.Y. McSween (eds) *Meteorites and the Early Solar System II*. Tucson, AZ: University of Arizona Press, 2006, pp.625–651.
48. G.J. Flynn, S. Wirick, L.P. Keller, C. Jacobsen. "Modification of the Murchison Insoluble Organic Matter (IOM) by Acid Extraction". *LPI Contributions. Abstract #5162*. 2010. Pp. 5162.
49. C.M.O.D. Alexander, R. Bowden, M.L. Fogel, K.T. Howard. "Carbonate Abundances and Isotopic Compositions in Chondrites". *Meteoritics Planetary Sci.* 2015. 50: 810–833.
50. J.R. Cronin, S. Pizzarello. "Aliphatic-Hydrocarbons of the Murchison Meteorite". *Geochim. Cosmochim. Acta.* 1990. 54: 2859–2868.
51. Y.J. Pendleton. "Detection of Organic Matter in Interstellar Grains". In: D.C.B. Whittet (ed.) *Planetary and Interstellar Processes Relevant to the Origins of Life*. Dordrecht, Netherlands: Springer, 1997, pp.53–78.
52. S.A. Sandford, L.J. Allamandola, A.G.G.M. Tielens, K. Sellgren, M. Tapia, Y. Pendleton. "The Interstellar CH Stretching Band near 3.4 Microns: Constraints on the Composition of Organic Material in the Diffuse Interstellar Medium". *Astrophys. J.* 1991. 371: 607–620.
53. Y.J. Pendleton, S.A. Sandford, L.J. Allamandola, A.G.G.M. Tielens, K. Sellgren. "Near-Infrared Absorption Spectroscopy of Interstellar Hydrocarbon Grains". *Astrophys. J.* 1994. 437: 683–696.
54. C.E. Amri, M.C. Maurel, G. Sagon, M.H. Baron. "The Micro-Distribution of Carbonaceous Matter in the Murchison Meteorite as Investigated by Raman Imaging". *Spectrochim. Acta A Mol. Biomol. Spectrosc.* 2005. 61: 2049–2056.
55. C.L. Guillou, S. Bernard, A.J. Brearley, L. Remusat. "Evolution of Organic Matter in Orgueil, Murchison and Renazzo During Parent Body Aqueous Alteration: In Situ Investigations". *Geochim. Cosmochim. Acta.* 2014. 131: 368–392.
56. L.D. Landau, E.M. Lifshitz, L.P. Pitaevskii. *Electrodynamics of Continuous Media*. Vol. 8, 2nd edition. Elmsford, New York: Pergamon Press, 1984.
57. T.W. Du Bosq, R.E. Peale, G.D. Boreman. "Terahertz/Millimeter Wave Characterizations of Soils for Mine Detection: Transmission and Scattering". *Int. J. Infrared Milli. Waves.* 2008. 29: 769–781.
58. H. Dehghani, B.W. Pogue, S.P. Poplack, K.D. Paulsen. "Multiwavelength Three-Dimensional Near-Infrared Tomography of the Breast: Initial Simulation, Phantom, and Clinical Results". *Appl. Opt.* 2003. 42: 135–145.

59. B. Recur, A. Younus, S. Salort, P. Mounaix, B. Chassagne, P. Desbarats, J.P. Caumes, E. Abraham. "Investigation on Reconstruction Methods Applied to 3D Terahertz Computed Tomography". *Opt. Express*. 2011. 19: 5105–5117.
60. B. Recur, J.P. Guillet, I. Manek-Honninger, J.C. Delagnes, W. Benharbone, P. Desbarats, J.P. Domenger, L. Canioni, P. Mounaix. "Propagation Beam Consideration for 3D THz Computed Tomography". *Opt. Express*. 2012. 20: 5817–5829.
61. L. Quaroni, M. Obst, M. Nowak, F. Zobi. "Three-Dimensional Mid-Infrared Tomographic Imaging of Endogenous and Exogenous Molecules in a Single Intact Cell with Subcellular Resolution". *Angew. Chem. Int. Ed.* 2015. 54: 318–322.
62. J.P. Guillet, B. Recur, L. Frederique, B. Bousquet, L. Canioni, I. Manek-Hönninger, P. Desbarats, P. Mounaix. "Review of Terahertz Tomography Techniques". *Journal of Infrared, Millimeter and Terahertz Waves*. 2014. 35: 382.
63. X.C. Zhang. "Three-Dimensional Terahertz Wave Imaging". *Phil. Trans. R. Soc. Lond. A*. 2004. 362: 283–298.
64. J. Nath, D. Panjwani, F. Khalizadeh-Rezaie, M. Yesiltas, E.M. Smith, J.C. Ginn, D.J. Shelton, C. Hirschmugl, J.W. Cleary, R.E. Peale. "Infra-red Spectral Microscopy of Standing-Wave Resonances in Single Metal-Dielectric-Metal Thin-Film Cavity". *Proc. SPIE*. 2015. 9544: 95442M.
65. D. Panjwani, M. Yesiltas, S. Singh, E.D. Barco, R.E. Peale, C. Hirschmugl, J. Sedlemair. "Patterning of Oxide-Hardened Gold Black by Photolithography and Metal Lift-Off". *Infrared Phys. Technol.* 2014. 62: 94–99.
66. E.M. Smith, D. Panjwani, J. Ginn, A.P. Warren, C. Long, P. Figuieredo, C. Smith, J. Nath, J. Perlstein, N. Walter, C. Hirschmugl, R.E. Peale, D. Shelton. "Dual Band Sensitivity Enhancements of a Vox Microbolometer Array Using a Patterned Gold Black Absorber". *Appl. Opt.* 2016. 55: 2071–2078.